NAVAL POSTGRADUATE SCHOOL
MONTEREY, CALIF. 93940

NAVAL POSTGRADUATE SCHOOL
Monterey, California

THESIS

CALCULATION OF THE OXIDE GROWTH RATE OF 2-1/4 Cr - 1 Mo STEEL IN AIR AND THE SUBSEQUENT MEASUREMENT OF THE STRAIN REQUIRED TO CRACK THE OXIDE

by

Robert Lawrence Langdon

September 1980

Thesis Advisor: K. D. Challenger

Approved for public release; distribution unlimited.

T196170

SECURITY CLASSIFICATION OF THIS PAGE (When Data Entered)

REPORT DOCUMENTATION PAGE

READ INSTRUCTIONS BEFORE COMPLETING FORM

1. REPORT NUMBER	2. GOVT ACCESSION NO. / 3. RECIPIENT'S CATALOG NUMBER
4. TITLE (and Subtitle): Calculation of the Oxide Growth Rate of 2-1/4 Cr - 1 Mo Steel in Air and the Subsequent Measurements of the Strain Required to Crack the Oxide	5. TYPE OF REPORT & PERIOD COVERED: Master's Thesis; September 1980
	6. PERFORMING ORG. REPORT NUMBER
7. AUTHOR(s): Robert Lawrence Langdon	8. CONTRACT OR GRANT NUMBER(s)
9. PERFORMING ORGANIZATION NAME AND ADDRESS: Naval Postgraduate School, Monterey, California 93940	10. PROGRAM ELEMENT, PROJECT, TASK AREA & WORK UNIT NUMBERS
11. CONTROLLING OFFICE NAME AND ADDRESS: Naval Postgraduate School, Monterey, California 93940	12. REPORT DATE: September 1980
	13. NUMBER OF PAGES: 68
14. MONITORING AGENCY NAME & ADDRESS(if different from Controlling Office): Naval Postgraduate School, Monterey, California 93940	15. SECURITY CLASS. (of this report): Unclassified
	15a. DECLASSIFICATION/DOWNGRADING SCHEDULE

16. DISTRIBUTION STATEMENT (of this Report)

Approved for public release; distribution unlimited.

17. DISTRIBUTION STATEMENT (of the abstract entered in Block 20, if different from Report)

18. SUPPLEMENTARY NOTES

19. KEY WORDS (Continue on reverse side if necessary and identify by block number)

2-1/4 Cr - 1 Mo Steel
Oxide Strain Tolerance
Oxide Growth Rate
Oxide Cracking
Oxide Spalling

20. ABSTRACT (Continue on reverse side if necessary and identify by block number)

This study examined the oxide growth rate of 2-1/4 Cr - 1 Mo steel in air under isothermal growth conditions. Two oxidizing temperatures were used, 403°C and 499°C, for five specimens each with oxidizing times varying from six hours to 700 hours. Average oxide growth rate as a function of time and temperature was found to be rate = $2.10 \times 10^{-3} \exp \frac{-12950}{RT}$ whereas maximum

DD FORM 1 JAN 73 1473 (Page 1) EDITION OF 1 NOV 65 IS OBSOLETE S/N 0102-014-6601

SECURITY CLASSIFICATION OF THIS PAGE (When Data Entered)

oxide growth rate corresponds to rate = $4.50 \times 10^{-3} \exp \frac{-13520}{RT}$. These values were found to be in general agreement with the limited data available in the literature.

The second part of the experiment related to the measurement of the strain required to crack the oxide. Discrete surface strains were imparted to oxidized specimens via a four-point-bend straining apparatus. The strained specimens were optically scanned for cracks with a stereoscope microscope capable of 70X magnification. A process of crack decoration was employed to enhance crack visibility. Because of certain equipment limitations, however, only an upper limit of strain tolerance could be determined. Methods of improving strain tolerance measurements are discussed.

Approved for public release; distribution unlimited.

Calculation of the Oxide Growth Rate of 2-1/4 Cr - 1 Mo Steel in Air and the Subsequent Measurement of the Strain Required to Crack the Oxide

by

Robert Lawrence Langdon
Major, Canadian Armed Forces
B.Sc., Sir George Williams University
Montreal, Quebec, Canada, 1973

Submitted in partial fulfillment of the
requirements for the degree of

MASTER OF SCIENCE IN ENGINEERING SCIENCE

from the

NAVAL POSTGRADUATE SCHOOL
September 1980

ABSTRACT

This study examined the oxide growth rate of 2-1/4 Cr - 1 Mo steel in air under isothermal growth conditions. Two oxidizing temperatures were used, 403°C and 499°C, for five specimens each with oxidizing times varying from six hours to 700 hours. Average oxide growth rate as a function of time and temperature was found to be rate = 2.10×10^{-3} $\exp \frac{-12950}{RT}$ whereas maximum oxide growth rate corresponds to rate = 4.50×10^{-3} $\exp \frac{-13520}{RT}$. These values were found to be in general agreement with the limited data available in the literature.

The second part of the experiment related to the measurement of the strain required to crack the oxide. Discrete surface strains were imparted to oxidized specimens via a four-point-bend straining apparatus. The strained specimens were optically scanned for cracks with a stereoscope microscope capable of 70X magnification. A process of crack decoration was employed to enhance crack visibility. Because of certain equipment limitations, however, only an upper limit of strain tolerance could be determined. Methods of improving strain tolerance measurements are discussed.

TABLE OF CONTENTS

I. INTRODUCTION - 9

A. BACKGROUND - - - - - - - - - - - - - - - - - - 9

B. THESIS OBJECTIVE - - - - - - - - - - - - - - - 15

II. EXPERIMENTAL PROCEDURE - - - - - - - - - - - - - - 19

A. GENERAL- 19

B. LITERATURE SEARCH FOR EXPECTED OXIDE MORPHOLOGY - - - - - - - - - - - - - - - 20

C. TEMPERATURE MEASUREMENT- - - - - - - - - - - - 21

1. Thermocouple Calibration - - - - - - - - - 21

2. Furnace Control- - - - - - - - - - - - - - 22

D. STRAINING APPARATUS- - - - - - - - - - - - - - 23

E. EXPERIMENTAL TRIAL - - - - - - - - - - - - - - 25

1. Initial Trial- - - - - - - - - - - - - - - 25

2. Metallographic Mounting and Polishing Technique- - - - - - - - - - - - 27

3. Crack Decoration - - - - - - - - - - - - - 28

F. FINALIZED EXPERIMENTAL PROCEDURE - - - - - - - 29

III. EXPERIMENTAL RESULTS - - - - - - - - - - - - - - - 30

IV. DISCUSSION - 33

V. CONCLUSIONS- 46

VI. RECOMMENDATIONS FOR FUTURE WORK- - - - - - - - - - 47

APPENDIX A - THEORETICAL CALCULATION OF THERMAL STRESSES IN A MULTI-LAYERED OXIDE - - - - 48

BIBLIOGRAPHY - 65

INITIAL DISTRIBUTION LIST- - - - - - - - - - - - - - - 68

LIST OF TABLES

Table		Page
I	Surface Strain Correction Factors- - - - - - -	51
II	Thermal Expansion Coefficients Used for Calculation of Mismatch Strains- - - - - -	52
III	Specimen Identification - Growing Times and Temperature- - - - - - - - - - - - - - - - -	53
IV	Oxide Thickness- - - - - - - - - - - - - - - -	54
V	Strain Tolerance - - - - - - - - - - - - - - - -	55

LIST OF FIGURES

Figure		Page
1	Specimen Sample Used for Furnace Temperature Fluctuation Determination	56
2	Straining Apparatus and Strain Indicator	57
3	Geometry of Straining Apparatus	58
4	Oxide Delamination 499°C Specimen	59
5	Oxide Layer 403°C Specimen	60
6	Tensile Surface Cracking	61
7	Compressive Surface Spalling	61
8	Tensile Surface Cracking	62
9	Average Oxide Thickness vs. Time	63
10	Comparison of Experimentally Determined Rate Constants with Published Data	64

ACKNOWLEDGEMENT

I wish to express my deep appreciation to Professors K. D. Challenger and M. Edwards for their expert guidance and assistance; to Mr. Ken Mothersell and staff of the Mechanical Engineering machine shop for their prompt preparation of experimental materials and apparatus; to Mr. Tom Kellogg for his willing laboratory assistance; and finally to Dr. M. Manning of the Central Electricity Research Laboratories, Surrey, England, for the up-to-date literature he sent. Without the strong and willing support of the above individuals, timely completion of this thesis would have been difficult if not impossible.

I. INTRODUCTION

A. BACKGROUND

In order to meet the electrical and energy needs of the 1980's, it will probably be necessary to draw power from nuclear energy sources. With growing public concern about nuclear reactors, it is of paramount importance that a proven, environmentally safe, commercial breeder system be developed. Conventional water-cooled reactors cannot meet the energy requirements of the future because of their dependence upon U^{235} uranium which comprises about .7% of uranium oxide which itself is scarce and non-renewable. The remainder of uranium oxide is essentially U^{238} of which there is currently more than 250,000 tons stockpiled in the United States alone [Ref. 1]. The technology exists in the form of a Liquid Metal Fast Breeder Reactor (LMFBR) which can convert the stockpiles of U^{238} uranium to a plutonium fuel and thus produce more than 50 to 60 times the energy from the same amount of uranium oxide that current light-water reactors do. Such a reactor is scheduled to be built in the United States near the Clinch River in Oak Ridge, Tennessee, and has been officially designated the Clinch River Breeder Reactor Plant (CRBRP). The CRBRP, however, will not be a full-scale commercialized reactor plant but will be a scaled-down prototype model used to assess the environmental impact

of future breeder commercialization. A decision on commercialization of LMFBR's in the United States will not be made before 1986 by the Energy Research and Development Administration (ERDA) until environmental impact and other safety-related data are ascertained [Ref. 2].

One of the Department of Energy's major concerns with regard to LMFBR commercialization is proper material selection. Unlike the light-water reactors currently in use, LMFBR's will be cooled with pure sodium because of its high thermal conductivity, high boiling point and because it does not slow down the high energy neutrons needed for efficient breeding of plutonium fuel. The peak sodium outlet temperature will be 535°C compared to only 343°C in pressurized water reactors. The heat generated during nuclear fission is transferred by conduction to the sodium coolant along the fuel rods. The primary sodium coolant loop couples to a secondary sodium loop which transfers heat to a steam generator which, in turn, supplies steam to a steam-driven turbine. The primary-secondary sodium loop arrangement is designed to ensure that radioactive and chemically active sodium flowing through the core is isolated from the water in the steam generators [Ref. 1]. The high operating temperatures coupled with sodium's high thermal conductivity and its potential, if mixed with water, to cause stress corrosion cracking in most structural materials makes proper

material selection vital to the safe operation of LMFBR's. For any material selected, it is essential that its mechanical properties be well characterized to ensure fully safe operation for the design life of the reactor -- some 210,000 hours [Ref. 3].

On the basis that 2-1/4 Cr - 1 Mo alloy steel is compatible with both liquid sodium and steam, and on the fact that this material is accepted for both Section III (Nuclear) and Section VIII (Pressure Vessel) applications of the ASME Boiler and Pressure Vessel Code [Ref. 4], it was selected as one of the reference materials for use in the prototype steam generators at CRBRP [Ref. 3]. Although used for many years in conventional steam boiler operations, there has been little requirement to closely evaluate the high temperature properties of 2-1/4 Cr - 1 Mo steel. In steam boilers, the heat transfer across the fire/metal interface is considerably less efficient than will be the heat transfer across the liquid sodium/metal interface in LMFBR's. Because of the relatively poor heat transfer in steam boilers, conservatively thick metal plate and tubing are used to counteract severe fireside corrosion without significantly reducing the overall boiler efficiency. In LMFBR's, however, because of the excellent heat transfer properties of liquid sodium, such conservatism would significantly reduce the overall design efficiency. Further, sodium is an innocuous enviornment

as far as corrosion is concerned. For these reasons, 2-1/4 Cr - 1 Mo steel in LMFBR's will be used close to its design limits. This fact dictates that its high temperature properties be accurately assessed.

One area of major concern is the high temperature fatigue life of 2-1/4 Cr - 1 Mo steel. The efficient heat transfer properties of liquid sodium will result in thermal gradients in the steam generators which will product large thermally induced stresses via thermal expansion and contraction. Repeated application of these stresses caused by thermal fluctuations in the system, combined with operating stresses, leads to a combined fatigue and creep loading which interacts synergistically to produce failure in a time much less than that which would be predicted by a linear summation of the fatigue and creep damage. This concern, therefore, has prompted several studies over the last few years in an attempt to mathematically quantify the high temperature fatigue characteristics of 2-1/4 Cr - 1 Mo steel [Refs. 5 and 6]. These studies, however, although adding significantly to the available knowledge of 2-1/4 Cr - 1 Mo steel, have not been successful in producing adequate design correlations which accurately predict fatigue failure of this alloy at high temperatures [Ref. 7]. (Fatigue life is dependent upon crack initiation and crack growth per cycle. For austenitic steels, at least, both crack initiation and crack growth at

elevated temperatures are enhanced by grain boundary voids formed by creep during unbalanced fatigue cycling resulting in the creep-fatigue interaction, CFI [Ref. 8].)

Challenger, Miller and Brinkman [Ref. 9] attribute the lack of success in obtaining adequate design correlations for 2-1/4 Cr - 1 Mo steel to a general misunderstanding of the CFI mechanism in this alloy. They note that 2-1/4 Cr - 1 Mo steel in CFI testing often fails by transgranular crack initiation and growth whereas, if creep damage alone were responsible for reduced fatigue life at high testing temperatures, that failure would occur by intergranular crack initiation and growth. All studies recognize that hold periods in the normal continuous cycle fatigue hysteresis loop reduce the fatigue life of 2-1/4 Cr - 1 Mo steel at elevated temperatures and attribute this to a loss in interaction solid solution hardening (ISSH). ISSH is a result of dynamic strain aging involving interaction between molybdenum and carbon atoms, or atom clusters, with dislocations prior to the precipitation of an eventually stable metal carbide precipitate [Ref. 10]. Its effects on the creep and rupture behavior of 2-1/4 Cr - 1 Mo steel have been documented by Klueh [Ref. 11]. At the high temperatures, precipitation is much faster, resulting in a loss of dynamic strain aging effects. This fact alone, however, does not account for the total decrease in fatigue life at high temperatures.

Challenger et al. hypothesize that the reduction in fatigue life with hold periods in the hysteresis loop is enhanced more by an environment fatigue interaction than by CFI. At the higher temperatures, oxidation takes place, resulting in an oxide film on the metal surface. Fatigue cycling results in cracks in the oxide which serve as fatigue crack initiation sites, thereby reducing total fatigue life which, as previously stated, is comprised of cycles to initiate the crack and cycles for crack propagation. Having more easily initiated crack sites (oxide cracks) therefore reduces total fatigue life. Further, the reduction in fatigue life would be even greater for high-cycle fatigue where a greater portion of the total cycles to failure is spent in crack initiation. Hold periods in compression would be more damaging than hold periods in tension because the oxide would experience maximum tensile strain on cycle completion and would crack perpendicular to the direction of maximum tensile strain. (If formed during a tensile hold period, the maximum tensile strain in the oxide on subsequent compression would be $\nu\Delta\varepsilon_T$ where ν is Poisson's ratio and $\Delta\varepsilon_T$ is the total strain range for the test. Any resultant oxide cracks would be parallel to the compressive strain direction; such axial cracks would not affect fatigue crack initiation.) All the available literature on CFI interaction analyzed by Challenger et al. substantiates their

hypothesis regarding environment-fatigue interaction. To further justify their hypothesis, however, they had Oak Ridge National Laboratory perform a zero-stress hold period test at 538°C following the maximum compressive strain. At zero stress, the CFI mechanism would not be apparent (no creep damage at zero stress). Yet fatigue life of the material was still significantly reduced from the expected fatigue life had it been continuously cycled. Only an environment fatigue interaction can explain this result, thereby strongly supporting their hypothesis [Ref. 10].

B. THESIS OBJECTIVE

In a second paper, Challenger and Miller formulated a mathematical correlation to predict the effects of hold periods on fatigue life at elevated temperatures for 2-1/4 Cr - 1 Mo steel based on environment fatigue interaction [Ref. 12]. Although their correlation proved to be more accurate than other correlations (primarily CFI correlations) proposed to account for reduced fatigue life under high temperature fatigue cycle hold period conditions, they note that it is based on several assumptions which require experimental verification. The aspects which require additional experimental verification are:

1. The total number of cycles to failure for low strain range continuously cycled tests without any enhancement due to ISSH.

2. Verification of the oxidation rate of 2-1/4 Cr - 1 Mo steel in air. (For their correlation, they used

data from a Nuclear Systems Material (NSM) Handbook [Ref. 13] which describes the oxidation rate of 2-1/4 Cr - 1 Mo in air in terms of metal loss, m, where

$$m = \frac{2.404 \times 10^{-2}}{\rho} \exp \frac{-14759}{RT} t^{1/2} ;$$

ρ = density of iron; R = gas constant; T = temperature in K; and t = time in hours. From this expression, they calculated oxide thickness, h, as a function of time at temperature as

$$h = 6.16 \times 10^{-3} \exp \frac{-14759}{RT} t^{1/2}$$

where R = gas constant; T = K; t = time in hours.)

3. Verification of the relationship between oxide thickness and fracture strain of the oxide. (For their relationship they used Manning and Metcalfe's relationship [Ref. 14],

$$\varepsilon_f^{\circ} > \left(\frac{\gamma'}{hE}\right)^{1/2}$$

derived by comparing the energy required to generate new surface by delamination, with the energy stored in the oxide when strained, where ε_f° = strain in the oxide; γ' = a parameter proportional to shear fracture surface energy density, experimentally determined by fitting spalling data to the criterion; E = the elastic modulus of the oxide; and h = oxide thickness in meters.

4. The relationship between strain range and the number of cycles required to initiate a fatigue crack in the absence of oxide cracking. For correlation purposes, they assumed that a crack in the oxide perpendicular to the applied stress is considered to be identical to a crack of similar dimensions in the metal itself. In the absence of oxide cracking, crack initiation is related to plastic strain and as such is influenced by the slip character of the material. Without data on 2-1/4 Cr - 1 Mo steel, they used Mayia's relationship [Ref. 15] $\frac{N_n}{N_f}$ for 304 stainless steel because of slip character similarities and transgranular fatigue crack

initiation. N_n = number of cycles to crack initiation; N_f = number of cycles to failure.

5. The effect of hold period and wave form on fatigue crack propagation rate. Combined tensile and compressive hold periods had a greater detrimental effect on fatigue life than compressive hold periods alone. They believe that once a crack has been initiated, tensile hold periods hold the crack open for further oxidation and enhance fatigue life reduction through environmental interaction. If possible, this enhanced crack growth rate and environmental interaction should be quantified or at least verified.

The purpose of this thesis is to experimentally verify the oxidation rate of 2-1/4 - 1 Mo steel in air and subsequently to verify the relationship between oxide thickness and fracture strain of the oxide. It is hoped that this will add in some small part to the United States Department of Energy's eventual approval for commercialization of LMFBR's. Further, and although not previously mentioned, problems are being encountered in current power generation boilers where super-heater and reheater tubes, many of which are made from 2-1/4 Cr - 1 Mo steel, are experiencing scale blockages because steam-side oxidation releases scales into the steam circuit. Even where oxide scale release is not sufficient to cause blockages, the introduction of oxide scale into the steam circuit has been found to cause erosion of turbine blades [Ref. 16]. Calculation of the strain tolerance of the oxide which should decrease with increasing oxide thickness (see Manning's relationship, page 16) and therefore operating time, and knowing oxide growth rates, should

prove beneficial in establishing periodic maintenance schedules for de-scaling operations where the oxide could be chemically removed before it spalls.

II. EXPERIMENTAL PROCEDURE

A. GENERAL

The absence of standard experimental procedures for the measurement of oxidation rates and oxide strain tolerance testing necessitated the formulation of suitable evaluation methods. To formulate these, the following was considered:

1. A literature search would have to be made to determine expected oxide morphology as a function of growing temperature. If the same oxide would form at higher temperatures (above 535°C) as would be formed at or below 535°C, and assuming that growth rate was parabolic as would be expected in a diffusion controlled process; then it would be preferred to grow the oxide at higher temperatures because shorter times for the same oxide thickness would be required.

2. Again assuming oxidation to be an Arrhenius controlled process with solution of the form:

$$\text{Rate} = A \exp\left(\frac{-\Delta E}{RT}\right)$$

with A being a constant for the particular process; ΔE the activation energy; R the gas constant; and T the temperature in Kelvins; as would be expected in a thermally activated (diffusion controlled) process, then establishment of accurate temperature controls and fluctuation limits would be important. (The solution varies exponentially with temperature.) Further, to find values for A and $\frac{-\Delta E}{R}$ a minimum of two growing temperatures would be required as the solution would take the form of

$$\ln \text{Rate} = \ln A - \frac{\Delta E}{RT}$$

wherein a plot of ln Rate versus $\frac{1}{T}$ would yield slope $-\frac{\Delta E}{R}$.

3. In order to measure the subsequent strain to crack the oxide, some combination of straining apparatus and

optical magnification system would be required. In this regard, it would be preferred if the strain could be applied in increments rather than dynamically as it would take time to optically search the specimen for cracks at various strain levels.

4. Prior to conducting the actual experiment, a trial run should be conducted to verify the designed experimental procedure and apparatus.

B. LITERATURE SEARCH FOR EXPECTED OXIDE MORPHOLOGY

Reviewing the literature to determine expected oxide morphology of 2-1/4 Cr - 1 Mo steel oxidized in air as a function of temperature proved to be frustrating as no pertinent data could be found. All available literature pertaining to the oxidation of 2-1/4 Cr - 1 Mo steel concerned oxidation in a steam environment [Refs. 16 - 19]. Even this data was somewhat limited because, as noted by Griess et al. [Ref. 19], there has been little incentive to quantitatively determine corrosion rates of low alloy steels in steam because when they are used in conventional fossil-fired power plants, steam -side corrosion is insignificant when compared to fire-side corrosion. It has only been in the last decade or so that much attention has been paid to steam-side corrosion because of the scale blockage problems being encountered in the super-heater and reheater tubes of the modern generation boilers.

The above notwithstanding, the following facts led to the decision not to use oxidizing temperatures greater than 500°C:

1. 2-1/4 Cr - 1 Mo steel oxidizes in steam to form a duplex oxide scale with the inner layer consisting of a mixed spinel containing alloying elements and some of the iron $(Fe, Cr)_3O_4$ and an outer layer of Fe_3O_4 (in scales removed from operational super-heaters the outer layer contained limited amounts of the higher oxide Fe_2O_3 but usually under laboratory conditions little Fe_2O_3 formed due to low oxidation potentials) [Ref. 14]. Each layer was approximately of equal thickness and under isothermal growth conditions generally remained adherent and free of cracks for growing periods exceeding 4000 hours [Ref. 19].

2. Oxide morphologies representative of long-term oxidation at lower temperatures can be grown by short-term oxidation in steam at 650-700°C; however, cracks due to thermal mismatch alone (see below) were revealed on oxides on a 9% Cr steel cooled from 650°C [Ref. 14].

3. Aside from mechanically imposed strains, the strain which leads to oxide cracking is generally caused by thermal expansion coefficient mismatches between the metal and the oxide on cooling.

$$\varepsilon_c = (T_1 - T_2)(\alpha_m - \alpha_u)$$

where ε_c is the cooling strain; $(T_1 - T_2)$ is the temperature drop; and α_m and α_u are the expansion coefficients of the metal and oxide. The thermal expansion coefficients, however, depend on their lattice parameters which are temperature-dependent. Thermal expansion coefficient relations for iron and its oxides as a function of their lattice parameter at elevated temperatures were determined by Gorten et al. [Ref. 20]. However, for Fe_3O_4 they note that their lattice parameter relationship is invalid between 500-700°C because of a magnetic transformation at its Curie temperature of 588°C which affects lattice size over the range indicated.

C. TEMPERATURE MEASUREMENT

1. Thermocouple Calibration

In order to be able to accurately measure temperature, the first requirement was for a calibrated thermocouple

and temperature readout. A chromel-alumel thermocouple was made and attached to a digital temperature reader. 99.999% pure aluminum and 99.999% pure bismuth with melting temperatures of 660.1°C and 271.4°C, respectively, were used as standards. These were melted and their respective freezing points were measured using the prepared thermocouple and reader. It was found that over this temperature range, temperatures were measured 0.5% low. For all subsequent temperature measurements, this correction factor was used.

2. Furnace Control

Three Hoskins electric furnaces, type F202C with a heating box 9" (22.8 cm) deep, 5" (12.7 cm) wide, and 4-1/2" (11.4 cm) high were wired and set at respective temperatures of 350°C, 425°C and 530°C. A thermocouple was inserted and the digital readout was linked to a recorder to measure temperature fluctuation. The furnaces showed a maximum fluctuation over a 24-hour period of only ±2°C which was considered satisfactory. Front-to-back temperature variation was then measured on one of the furnaces using a suspended specimen sample with five thermocouples welded directly on it as indicated in Figure 1. Front-to-back temperature varied more than 30°C over the 5-1/2" (14 cm) specimen length. This temperature variation would have been too great for experimental purposes so use of the Hoskins electric furnace was abandoned.

Temperature fluctuation and front-to-back temperature variation were measured on three much bigger Linberg Hevi Duty furnaces using the procedures described above. These proved to be satisfactory for experimental purposes having a maximum fluctuation of ±2°C over a 24-hour period with a variation of only 3°C over the 5-1/2" (14 cm) specimen length. (The test specimen had been placed longitudinally in the furnace with the deepest thermocouple located approximately 2" (5 cm) from the back wall.)

D. STRAINING APPARATUS

Figure 2 shows the straining apparatus which was designed to impart measurable amounts of strain to the surface oxide grown on specimens. The specimen when clamped to the bending arms of the rig lies on the bearing axis. One pivot block is mounted on ball bearings so that, when equal amounts of weights are suspended from the bearing arms, the specimen can assume its natural length while bending. Hence only a pure bending moment is applied. Surface strain, or the strain imparted to the oxide is calculated from the center deflection of the specimen as follows:

(1) The maximum stress at the outermost fibers, $\sigma \text{ max} = \frac{Mc}{I} = E\varepsilon$ [Ref. 21] where M is the internal bending moment; I the moment of inertia of the section about the neutral axis; E is the modulus of elasticity; ε is the surface strain; and c is the distance from the outermost

fiber to the neutral axis ($c = \frac{h}{2}$ where h is the specimen thickness).

(2) The linear equation relating the radius of curvature R to the internal bending moment M is given by [Ref. 22] $\frac{1}{R} = \frac{M}{EI}$.

(3) Combining (1) and (2) get

$$\varepsilon = \frac{h}{2R} .$$

(4) R is found from the straining rig geometry as follows: (See diagram in Figure 3.)

(a) The center portion of the specimen of length L under uniform bending assumes radius R. From the relationship that $L = R\theta$ [Ref. 29] get $\frac{\theta}{2} = \frac{L}{2R}$.

(b) From geometric configuration, get

$$\delta = R(1 - \cos \frac{L}{2R}) + \ell \sin \frac{L}{2R} .$$

(c) Assume small values of $\frac{L}{2R}$ and approximate to

$$R = \frac{L^2(1 + \frac{4\ell}{L})}{8\delta} .$$

(d) Substitute into equation (3) to get

$$\varepsilon = \frac{4\delta h}{L^2(1 + \frac{4\ell}{L})}$$

In the actual experiment $\frac{L}{2R}$ is not small because of the fact that the specimen used was only .030" (.762 mm) thick, and a large deflection had to be imposed to get even relatively small strains. To correct for the inaccuracy of assuming small $\frac{L}{2R}$ actual strain as measured by a strain gauge was compared with measured δ. See Table I for correction factors.

E. EXPERIMENTAL TRIAL

1. Initial Trial

5-1/2" (14 cm) long, .030" (.762 mm) thick specimens were used for the experimental trial run. They were surface polished using 400-grit SiC paper; degreased with successive washings in zylene, acetone and alcohol with each wash being allowed to dry before the next wash was carried out; and finally suspended in the Linberg furnaces at oxidation temperatures of 474°C and 322°C.

A specimen from the 474°C furnace was removed after 22 hours, but the oxide spalled on air cooling. The spalled scale was magnetic indicating that it was $(Fe,Cr)_3O_4$ or (Fe_3O_4) or a combination of both. The cooling strain on the oxide was calculated using the following relationships derived by Gorten et al. [Ref. 20].

$$\alpha_i = \frac{1}{a_o(T)} \frac{da_o}{dT}$$

where $a_o(T)$ oxide $= 8.3939 + 8.46 \times 10^{-5} T + 5.51 \times 10^{-9} T^2$ and $\Delta\varepsilon_c = (T_1 - T_2)(\alpha_m - \alpha_o)$. See Table II for tabulated thermal expansion coefficients.

The cooling strain is a summation of incremental strains on cooling. For example,

$$(474 - 450)(\alpha_{m_{474}} - \alpha_{o_{474}}) + (450 - 400)(\alpha_{m_{450}} - \alpha_{o_{450}})$$

$$+ (400 - 350)(\alpha_{m_{400}} - \alpha_{o_{400}}) + \text{etc.}$$

This yielded $\varepsilon_c = -.0001914$ (a compression strain) which was considered to be too low to have caused the spalling. It was believed, therefore, that thermal shock resulting from a temperature differential through the oxide thickness may have caused the spalling. If so, this could be eliminated by furnace cooling.

A second specimen was removed from the 474°C furnace after 337 hours oxidizing time and was quickly transferred to another furnace wherein it was allowed to furnace cool. Despite furnace cooling, however, the oxide still spalled. It was assumed at this time that the spalling must have resulted from cooling strains, the small calculated strain notwithstanding. If this were true, then the strain to crack the oxide could be calculated by watching samples furnace cool from their oxidizing temperature to room temperature and recording the temperature at which spalling

occurred. Assuming this, new specimens were placed in another furnace at 494°C. It was thought that specimens with longer oxidizing times would spall first on cooling, and that others would spall at successively lower temperatures. This did not prove to be true as none of the specimens spalled, even though the expected oxide thicknesses bracketed those of the 474°C specimen which had spalled.

The only procedural difference between the 474°C specimens was in the degreasing procedure. In degreasing the latter specimens, the successive applications of zylene, acetone and alcohol had been rinsed off while wet. It was concluded, therefore, that improper degreasing procedures had led to the spalling of the 474°C specimens. For future experimental runs, degreasents were wiped dry.

2. Metallographic Mounting and Polishing Technique

Various mounting and polishing techniques were tried to polish the oxide and to prevent oxide cracking using the 322°C specimens which, despite improper degreasing techniques, had not spalled. Additionally the 494°C specimens were mounted and polished. These methods included nickel plating (would not plate over thick oxide); mounting in a metal clamp between two pieces of copper (could not prevent edge rounding); mounting the specimen in various mounting materials including bakelite, epoxy, plastimet and formvar with subsequent hand sanding through 240 to 600 grit paper

and/or six-micron diamond paste. No method proved satisfactory as either edge rounding or more probably oxide fracture caused by the specimen flexing in the mount invariably occurred. To preclude specimen flexing, thicker specimens, .081" (2.057 mm) thick, were oxidized and the various mounting and polishing techniques were again tried. Although the tendency for the oxide to break from the mount was significantly reduced, edge rounding still precluded good resolution of the oxide layer. It was found though that automatic polishing for several hours on the vibromet following mounting in formvar and hand polishing with three-micron diamond paste led to satisfactory oxide resolution. This was the technique used for experimental verification of oxide thickness. (Due to the non-availability of sufficient .81" (2.057 mm) thick 2-1/4 Cr - 1 Mo steel, it was necessary to still use the .030" (.762 mm) specimens for bending tests. To ensure equal oxide growth, thick and thin specimens were co-mounted prior to eventual oxidation.)

3. Crack Decoration

Specimens from the 322°C and 494°C trial runs were bent in the straining apparatus and were microscopically scanned at various intervals. The limited magnification of the stereoscope microscope, however, (70X) did not reveal oxide cracks before spalling occurred. Partially spalled

samples were electrolytically plated with copper and were rescanned. Cracks normal to the applied strain were now revealed because of this crack decoration process. Such crack decoration was used in the final experimental procedure. The plating solution had been prepared using 15 gms of $CuSO_4$ dissolved in 100 ml of distilled water mixed with 5 ml of H_2SO_4 in 100 ml of distilled water. The bath potential used varied between one and three volts.

F. FINALIZED EXPERIMENTAL PROCEDURE

The revised experimental procedures were as follows:

1. 1" (2.54 cm) long, .081" (2.07 mm) thick specimens, and 3" (7.62 cm) long, .030" thick specimens, were surface polished using 400-grit paper; co-mounted; and degreased.

2. Co-mounted specimens were inserted into Linberg Hevi-Duty furnaces at various times at growing temperatures of 499°C and 401°C. See Table II for growing times and specimen identification.

3. At the end of the oxidation period, the furnaces were shut off and all specimens were allowed to furnace cool.

4. The .081" (2.07 mm) thick specimens were sections using the cut-off grinding wheel, mounted in formvar, hand polished through 240 to 600-grit paper, further hand polished in three-micron diamond paste using kerosene as a lubricant, automatically polished with a one-micron Al_2O_3 solution on the Vibromet polisher for up to 12 hours, and the respective oxide thicknesses were microscopically determined at a magnification of 1000X.

5. The .030" (.762 mm) specimens were placed in the straining apparatus and bent. The deflection was measured with an extensometer calibrated to .001" (25.4 mm). Following successive load applications, the specimen surface was scanned optically for evidence of cracks or spalling.

III. EXPERIMENTAL RESULTS

A. OXIDE MORPHOLOGY

1. Macroscopic

After the specimens had been allowed to furnace cool, they were removed from the furnace and examined. All specimens were covered with a loosely adherent, reddish brown oxide, assumed to be Fe_2O_3. The Fe_2O_3 had a greasy consistency and wiped off easily with cotton swabs. The under layer was black and apparently tightly adherent. No visual evidence of spalling of this underlying oxide could be found on any of the specimens.

2. Microscopic

The thicker specimens of each run were sectioned, mounted and polished, and examined microscopically at 1000X. In all cases, the oxide from the 499°C specimens contained cracks and/or voids and was delaminated from the metal surface. The delamination occurred near the metal/oxide interface but through the inner $(FeCr)_3O_4$ layer. (See Figure 4.) All oxide damage was assumed to have resulted from the polishing technique used as no apparent oxide cracks could be found microscopically on the thinner unmounted specimens even using the crack decoration technique. The oxide from the 403°C specimens for the most part adhered to the metal substrate. (See Figure 5.)

In all cases, there was a duplex oxide scale as had been found in steam experiments. For the specimens oxidized at 403°C, however, the two oxide layers were not of equal thickness, the inner layer invariably being thicker. (See Figure 5.)

B. OXIDE THICKNESS

Oxide thickness was determined microscopically at 1000X by taking 20 measurements each at regular intervals and averaging. Where the oxide had delaminated, the thickness of the delaminated oxide was added to the thickness of the residual oxide on the metal. Results are shown in Table IV. Also shown are the maximum and minimum thicknesses of each specimen.

C. STRAIN TOLERANCE

The oxidized thin specimens were mechanically strained in the bending apparatus. L, the specimen length between the clamps, was kept the same in all cases in order to use the strain correction factors of Table I and was equal to 2-1/64" ±1/64" (5.12 cm ± .04 cm). Results are shown in Table V.

For the 499°C specimens, with one exception (specimen 1-1), the surface in compression spalled off before any visible cracks became apparent on the surface in tension. Crack decoration, however, revealed that cracks perpendicular

to the applied strain on the tensile side of the specimens were present. (See Figure 6.) For specimen 1-1, however, the outer oxide layer spalled in very localized areas at almost the same time as the compressive surface layer spalled. No prior cracking had been visible at 70X. Crack decoration again revealed the presence of short cracks perpencicular to the direction of maximum tensile strain.

The manner of spalling from the compressive surface of the 499°C specimens was in all cases similar. The oxide broke off in longitudinal pieces. (See Figure 7.) Here the copper decorating technique has been used to accentuate the spalled area. Despite decoration, however, longitudinal cracks could not be found.

No cracks or spalling from any of the 403°C specimens were observed even at the maximum applied strain of .84%. Again, however, crack decoration revealed that the surface in tension indeed had been cracked. (See Figure 8.) The crack decoration technique caused the compressive surface layer to spall longitudinally as had been previously observed.

It is a surprising result that the compressive surface of the 403°C specimens did not spall whereas the compressive surface of the 499°C specimens had. The total compressive strain in the former specimens was greater than those of the 499°specimens.

IV. DISCUSSION

A. OXIDE MORHPOLOGY

As noted in Section III.A.2, the 403°C specimens did not form a dual oxide layer of equal thickness, but instead formed a dual oxide layer with the inner layer (assumed to be an $(FeCr)_3O_4$ spinel) being significantly larger than the outer layer (assumed to be Fe_3O_4). There are two possible hypotheses for this result:

1. In the 403°C specimens, a duplex layer of equal thickness did in fact form; however, some of the Fe_3O_4 layer transformed to Fe_2O_3. Assuming the oxidation potential of air to be .2, such a reaction is thermodynamically possible [Ref. 24]. Nothing, however, could be found with regard to the kinetics of the reaction. If this hypothesis were true, though, it would be necessary that the transformation of Fe_3O_4 to Fe_2O_3 be favored at lower temperatures to account for the different thickness ratios of the duplex layers at the different oxidizing temperatures.

   Results from oxidation in steam tend to support this argument [Ref. 16], but it may result from higher ionization of the steam at higher temperatures and resultant hydrogen dosing which would serve to decrease the oxidation potential, making the transformation of Fe_3O_4 to Fe_2O_3 less favorable at higher temperatures due to the lowering of the oxidation potential at elevated temperatures.

2. The different oxidizing temperatures produce a different oxide morphology or perhaps damaged oxide layers which dramatically influence diffusion through the layers. (The fact that observed oxide growth rates are inconsistent with diffusion coefficients and hence activation energies of oxygen ion diffusion or iron ion diffusion through stoichiometric Fe_3O_4 will be discussed later.)

Because, as will be borne out later, experimentally determined total oxide thickness results compare favorably with the limited results published in the literature, the second hypothesis appears to be the more likely. If the first hypothesis were invoked, it would be expected that the experimental oxide thickness results for the 403°C specimens would be less than other published reuslts as the thickness of the Fe_2O_3 layer was not considered in this experiment.

B. GENERAL RATE SOLUTION BASED ON AVERAGE OXIDE THICKNESS

The rate of oxide growth was determined by dividing the average oxide thickness of each specimen by the square root of the oxidizing time. This is consistent with the assumption of a parabolic growth rate. The average growth rate for each temperature was then determined by summing the oxide growth rates of each run and dividing by the number of specimens in the run. This yields average growth rates of 4.51990×10^{-7} m - $s^{-1/2}$ for the 499°C (772.2°K) run and 1.3629×10^{-7} , - $s^{-1/2}$ for the 403°C (767.2°K) run.

Assuming an Arrhenius solution of the form

$$\text{Rate} = A \exp \frac{-\Delta E}{RT} ,$$

and taking the natural logorithm of both sides to get $\ln \text{Rate} = \ln A - \frac{\Delta E}{R} (\frac{1}{T})$, values of R and T (absolute) were inserted to get the following two equations in two unknowns:

(1) $\ln 4.5199 \times 10^{-7} = \ln A - S \left(\frac{1}{772.2}\right)$

(2) $\ln 1.3629 \times 10^{-7} = \ln A - S \left(\frac{1}{676.2}\right)$

where $S = \frac{\Delta E}{R}$.

Solving simultaneously yields:

$$S = 6520$$

$$A = 2.10 \times 10^{-3} .$$

Putting these values back into the Arrhenius form and taking R = 1.986 gives the following rate equation for the oxidation of 2-1/4 Cr - 1 Mo steel in air:

$$\text{Rate} = 2.10 \times 10^{-3} \exp \frac{-12950}{RT} .$$

Oxide thickness, h, therefore, is:

$$h = 2.10 \times 10^{-3} \exp \frac{-12950}{RT} (t^{1/2}) .$$

C. GENERAL RATE SOLUTION BASED ON MAXIMUM OXIDE THICKNESS

As indicated in Table IV, there was a wide variation of oxide thickness on each specimen. Assuming that the strain to crack an oxide is a function of oxide thickness (see Section I.B.3), then it may be beneficial to know the maximum oxide growth rate. Using the same procedure as above, but

with maximum oxide growth rates, gives the following relationship as a function of time and temperature for the maximum oxide thickness:

$$h = 4.50 \times 10^{-3} \exp \frac{-13520}{RT} (t^{1/2}) .$$

D. VERIFICATION OF PARABOLIC GROWTH RATES

For the above calculations, growth rate of an oxide was assumed to be parabolic. To verify this assumption, the average oxide thickness of each specimen was plotted against the square root of its respective oxidizing time. (See Figure 9.) If the assumption is correct, such a plot should yield a straight line fit which it did. Via the method of linear regression using the Hewlett-Packard curve fitting program, which applies a least-squares fit to the data, a coefficient of determination of .99 was obtained for both curves. This implies an excellent fit of the data to a straight line and as such verifies that the oxide growth rates are parabolic.

E. COMPARISON OF AVERAGE OXIDE GROWTH RATE TO PUBLISHED LITERATURE DATA

To provide a comparison of the average experimentally determined oxide thickness with published literature data, Table IV was compared with data in the Nuclear Systems Materials Handbook [Ref. 13]. This handbook describes the oxidation rate of 2-1/4 Cr - 1 Mo steel in air in terms of

metal loss, m, as:

$$m = \frac{K}{\rho} t^{1/2}$$

where K = a scaling constant in mg cm^{-2} $hr^{-1/2}$ and t is the oxidizing time in hours, and ρ = the density of 2-1/4 Cr - 1 Mo assumed to be 7.8 gm/cm^3. As noted by Challenger et al. [Ref. 12], oxide thickness, h, resulting from a metal loss, m, is approximately 2m. Therefore, oxide thickness, h, as a function of K, ρ, and t is:

$$h = \frac{2K}{\rho} t^{1/2} .$$

Using the above relationship and the data of Table IV, the average experimentally determined values of K based on average oxide thicknesses were determined to be .176 and .0528 for 499°C and 403°C, respectively. These values were then inserted on a plot of log K vs. 1000/T, $°K^{-1}$ published in the NSM Handbook [Ref. 13] and reproduced in Figure 10 for comparison purposes. As can be seen, the experimentally determined values correspond favorably to the published data. (The addition of these two data points, therefore, augments the limited published literature data and should serve to provide a better basis for the mathematical correlation of K previously determined to be: $K = 2404 \exp \frac{-14759}{RT}$ where T = temperautre in K and R = the gas constant, 1.986 cal/mole K.

Further, the experimentally determined value of K at 403°C is of particular importance as it provides justification for the extrapolation of published data to significantly lower temperatures. Finally, as can be seen in Figure 10, the correlation developed in this study is a better fit to the data than the NSM Handbook correlation. (See the dotted line.)

F. OXIDE GROWTH RATE CONTROL

The oxide growth rate should be controlled by (a) the diffusion of oxygen ions through the oxygen sub-lattice, (b) the diffusion of iron through the iron sub-lattice, or (c) possibly by gaseous diffusion through the oxide. The activation energy for diffusion of oxygen ions through stoichiometric Fe_3O_4 has been experimentally determined to be 17000 ± 1650 cal/mole [Ref. 30]. Further, the diffusion coefficient of iron through stoichiometric Fe_3O_4 [Ref. 31] has been found to be 4×10^{-17} cm^2/sec at 400°C and 5×10^{-15} cm^2/sec at 500°C, giving an estimated activation energy of 50,000 cal/mole. The higher diffusion coefficient of iron suggests that the growth of the Fe_3O_4 film, therefore, would be controlled by the outward diffusion of iron rather than the inward diffusion of oxygen ions.

However, from this work and from the results published in Ref. 13, an activation energy of 12,000 to 15,000 cal/mole was found to be more consistent with the actual oxide growth

rate. From this, we can conclude that the oxide growth rate is not controlled by stoichiometric diffusion of iron through the iron sub-lattice as might be expected, but by either non-stoichiometric diffusion or by gaseous diffusion. More work should be conducted to determine the exact growth mechanism.

G. STRAIN TOLERANCE

1. General

Trying to get accurate measurements of the strain required to crack the oxide was difficult, if not impossible, with the apparatus used. Although the straining apparatus worked well, the use of the extensometer to measure the deflection precluded simultaneous optical scanning of the deflected specimen. The extensometer, therefore, had to be removed after each successive load application so that the specimen could be optically viewed for cracks. Removal of the extensometer each time resulted in a slightly increased deflection because it no longer forced down on the specimen. When it was replaced, it would again reduce the deflection. Although Table I accounts for the reduced deflection caused by the extensometer, there is no way to say what effect, if any, the specimen flexing may have had on the oxide.

Another, more serious problem with the apparatus resulted from the large deflection of the specimen. The extensometer range limit was only 1" (2.54 cm). To measure

deflections greater than one inch, the extensometer had to be repositioned by moving it up an inch. Although great care was taken to make this repositioning as accurate as possible, it introduced an additional source of experimental error. This source of error could have been obviated if either thicker specimens had been used or if a more versatile extensometer had been available.

A third problem which precluded accurate determination of the strain to crack the oxide was the limited optical magnification (max 70X) used to scan the surface. With this low magnification, it was not possible to see cracks without crack decoration. The crack decoration technique, however, although revealing the presence of cracks, proved to be damaging to the oxide. A case in point is specimen 2-2. After removing this specimen from the furnace, the crack decoration technique was tried to see if any cooling cracks were present. Before any plating on the surface could be observed, the oxide started to spall off to reveal a plated metal substrate. Apparently plating had been going on through possibly a porous oxide and this subsequent plating caused the oxide to spall. Based on this experience, it was decided not to try the crack decoration technique until either some evidence of cracking was apparent or until the maximum straining capability of the straining apparatus was reached. (Crack decoration would

have been tried periodically had more than one specimen from each oxidizing time and temperature been available. Unfortunately, this was not considered soon enough.) For the above reasons, the experimentally observed strains to crack the oxide as tabulated in Table V represent only one upper limit to the actual required strain.

2. Strain Tolerance in Compression

Manning showed that an oxide will fail in compression when the total stored strain energy in the oxide per unit area is greater than the shear fracture surface energy of the oxide per unit area [Ref. 17], i.e., when $hE\varepsilon^2 > \gamma'$ where h = oxide thickness, E = Young's Modulus of the oxide, ε = the total oxide strain and γ' = some constant proportional to the interfacial surface energy density. The total strain to cause oxide spalling in compression, therefore, was derived to be

$$\varepsilon > \left(\frac{\gamma'}{hE}\right)^{1/2} .$$

Theoretically, therefore, thicker oxides should fail in compression at a lower strain than thinner oxides. The fact that all the 499°C specimens spalled from the compressive surface on bending whereas even the thicker oxides from the 403°C specimens did not even at greater applied strains seems contrary at Manning's relationship. The result is even more surprising when residual thermal expansion strains in the two

oxide surfaces are considered. The 403°C specimens have a greater residual compressive strain at room temperature than do the 499°C specimens.

There are three possible explanations for this apparent inconsistency:

a. The morphology of the oxide growth at 499°C is different than that grown at 403°C. Compare Figures 4 and 5. In Figure 4, the 499°C specimen, the oxide is already delaminated at the surface whereas in Figure 5, the 403°C specimen, it is not. The earlier assumption that specimen preparation had caused this oxide damage may not be correct. If the delamination of the higher temperature oxide existed prior to bending, it may well have been expected to spall before the lower temperature oxide which had not delaminated. What may have caused this prior delamination behavior is not known.

b. The calculation of the residual cooling strains is incorrect. To calculate the thermal strain, only the strain between the metal substrate and an Fe_3O_4 oxide layer was considered. In this regard, and in the absence of any data on thermal expansion coefficients for the $(Fe,Cr)_3O_4$ oxide layer, it was assumed that the spinel layer would have the same thermal expansion coefficients as the Fe_2O_3 layer. Further, any strain caused by the Fe_2O_3 layer was not considered because it was so non-adherent and wiped off easily. Thermal stresses in a three- or multi-layered oxide would be different than those in a two-layered oxide [Ref. 26]. (See Appendix A for amplification.)

c. There are some phase transformation strains caused by the transformation of some of the Fe_3O_4 oxide to the Fe_2O_3. If, as hypothesized in paragraph A.1 of this section, the formation of Fe_2O_3 from Fe_3O_4 is favored at lower temperatures given the same oxidizing environment, then the total transformation strain in the lower temperature oxide would be greater in magnitude than that of the higher temperature oxide. To decrease the propensity for spalling in compression, however, this transformation strain would have to be tensile in nature. This, however, goes contrary to the literature [Ref. 16] in that increased

amounts of Fe_2O_3 tend to enhance the tendency for spalling.

Irrespective of the reason for the lack of compressive spalling from the 403°C specimens, the compressive spalling data from the 499°C specimens tends to support the theory that compressive spalling is a function of oxide thickness. With the exception of specimen 1-3, the total compressive strain to cause spalling decreases with increasing oxide thickness. The non-supportive compressive strain value for specimen 1-3 could well be a function of the inaccuracy in measuring δ. More data points, however, would be preferred to support any conclusive arguments in this regard.

3. Strain Tolerance in Tension

If the oxide is strained in tension, it cracks normal to the applied strain. (See Figures 6 and 8.) Fractures in tension occur at a certain strain caused by the extension through the scale of cracks originating from surface defects in the layer. When the flaw size is small compared with oxide thickness, the fracture equation for the propagation of an edge crack in simple tension is [Ref. 20]:

$$K_{Ic} = 1.12\, E\varepsilon_c \sqrt{\pi c}\ .$$

This, coupled with the Griffith crack theory [Ref. 28] where:

$$K_{Ic}^{\ 2} = 2\gamma E\ ,$$

gives $$2\gamma = (1.12)^2 \pi E \varepsilon_c^2 c$$

or $$\gamma \approx 2E \varepsilon_c^2 c$$

$$\varepsilon_c \approx \sqrt{\frac{.5\gamma}{Ec}}$$

where ε_c is the critical strain; γ = the fracture surface energy density; E = the elastic modulus of the oxide; and c is the depth of the initiating flaw.

The above represents a theoretical relationship for oxide cracking, but it is interesting to note that the critical strain to cause cracking is not a function of oxide thickness unless c, the flaw size, is somehow dependent upon oxide thickness. Clearly, c cannot exceed oxide thickness, but for thick oxides, there is no reason to suspect that c should have any direct relationship to the oxide thickness.

It seems more logical that the depth of an originating flaw would depend more on oxide morphology than on oxide thickness. If, for example, c depended upon oxide grain size and assuming oxide grain size to be a function of nucleation and growth which are temperature dependent, then there would be an oxide formation temperature where the strain to crack the oxide would be minimal because of increased grain size.

To verify the above hypothesis would require a much more elaborate straining and optical viewing system than was available in this experiment. Such a system would have to be capable of determining the actual onset of cracking at more accurately determined strains. Further, in order to determine oxide grain size, better metallographic techniques will have to be employed. Such techniques would probably have to entail electrochemical polishing and/or oxide etching.

V. CONCLUSIONS

1. 2-1/4 Cr - 1 Mo steel oxidizes in air to form a three-layered oxide with the outer layer consisting of Fe_2O_3, the middle layer of Fe_3O_4, and the inner layer a mixed spinel of $(Fe,Cr)_3O_4$.

2. The average oxide thickness of 2-1/4 Cr - 1 Mo steel oxidized in air can be determined from the following relationship:

$$h(\text{meters}) = 2.10 \times 10^{-3} \exp \frac{-12950}{RT} (t(\text{hrs}))^{1/2} .$$

3. The maximum oxide thickness of 2-1/4 Cr - 1 Mo steel oxidized in air is given by:

$$h = 4.50 \times 10^{-3} \exp \frac{-13520}{RT} (t)^{1/2} .$$

4. Oxide growth rate is not controlled by the stoichiometric diffusion of iron through the iron sub-lattice as would be expected.

5. The determination of the exact strain tolerance of the oxide will require significantly higher optical magnification than 70X to determine the onset of cracking.

VI. RECOMMENDATIONS FOR FUTURE WORK

1. The straining apparatus should be modified so that the deflection need not be measured by an extensometer. In this regard, it is recommended that an engineer's gauge be affixed to the side of the bending apparatus instead of using the extensometer.

2. Thicker bending specimens should be used which will reduce the amount of deflection required to impart the same surface strain. With smaller deflections, strain can be calculated more accurately.

3. Further experimentation is required to determine the tensile strain tolerance of the oxide. In this regard, more than one bending specimen should be oxidized at each time and temperature to allow for periodic use of the crack decoration technique which proved to be somewhat damaging to the specimen.

4. Separate experiments should be conducted to determine oxide morphology as a function of oxidizing temperature. Such experimentation should try to determine whether oxide delamination is caused by growth conditions or specimen preparation. Further, and assuming that accurate oxide strain tolerances can be determined, knowledge of oxide morphology may lead to a better understanding of oxide cracking in tension. This should also serve to define the oxide growth mechanism.

APPENDIX A

THEORETICAL CALCULATION OF THERMAL STRESSES
IN A MULTI-LAYERED OXIDE

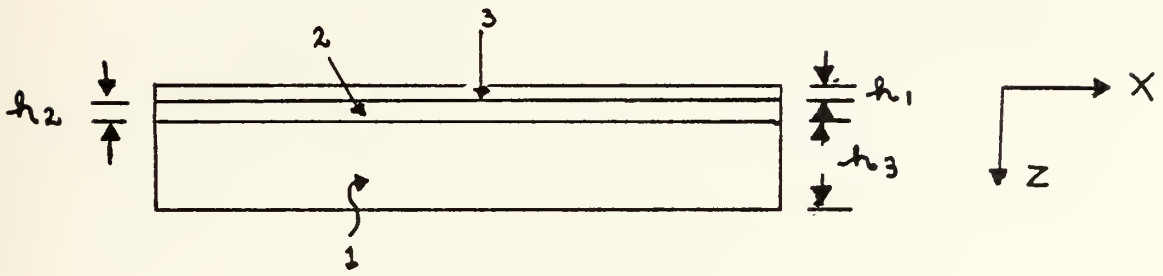

Three assumptions are required:

1. Materials are isotropic and linear.
2. Top layers are thin enough so that no flexure occurs.
3. There is a uniform temperature change, T, from unstressed state.

For any layer:

$$\varepsilon i = \varepsilon x_i = \varepsilon y_i = \frac{1 - \nu_i}{E_i} \sigma_i + \alpha_i \Delta T \quad . \qquad (1)$$

Also $\sigma_i = \sigma x_i = \sigma y_i$ and $\sigma z_i = 0$.

To maintain geometric compatibility:

$$\varepsilon_1 = \varepsilon_2 = \varepsilon_3 = \varepsilon \quad . \qquad (2)$$

Combine (1) and (2) to get

$$\sigma_i = \frac{E_i}{1 - \nu_i} (\varepsilon - \alpha_i T) \quad .$$

Equilibrium requires that:

$$\int \sigma dz = 0$$

$$\text{or} \quad \sum_{i=1}^{i=3} \frac{h_i E_i}{1 - \nu_i} (\varepsilon - \alpha_i T) = 0$$

$$\varepsilon = \frac{\Sigma \frac{h_i E_i \alpha_i}{1 - \nu_i}}{\Sigma \frac{h_i E_i}{1 - \nu_i}} \Delta T \qquad (3)$$

From (3) the strain in a three-layer oxide would be:

$$\varepsilon_{111} = \Delta T \left[\frac{\frac{h_1 E_1 \alpha_1}{1 - \nu_1} + \frac{h_2 E_2 \alpha_2}{1 - \nu_2} + \frac{h_e E_3 \alpha_3}{1 - \nu_3}}{\frac{h_1 E_1}{1 - \nu_1} + \frac{h_2 E_2}{1 - \nu_2} + \frac{h_3 E_3}{1 - \nu_3}} \right]$$

$$= \Delta T \left[\frac{(h_1 E_1 \alpha_1)(1-\nu_2)(1-\nu_3) + h_2 E_2 \alpha_2 (1-\nu_1)(1-\nu_3) + h_3 E_3 \alpha_3 (1-\nu_1)(1-\nu_2)}{h_1 E_1 (1-\nu_2)(1-\nu_3) + h_2 E_2 (1-\nu_1)(1-\nu_3) + h_3 E_3 (1-\nu_1)(1-\nu_2)} \right]$$

Simply by assuming $\nu_1 = \nu_2 = \nu_3$ to get

$$E_{111} = \Delta T \left[\frac{h_1 E_1 \alpha_1 + h_2 E_2 \alpha_2 + h_3 E_3 \alpha_3}{h_1 E_1 + h_2 E_2 + h_3 E_3} \right] . \qquad (4)$$

Similarly the strain in a two-layer oxide would be:

$$E_{11} = T \left[\frac{h_1E_1\alpha_1 + h_2E_2\alpha_2}{h_1E_1 + h_2E_2}\right] \quad . \qquad (5)$$

To get the difference in stress in any oxide layer, say the second layer, for example, substitute equations (4) and (5) into equation (3) and subtract:

$$(\sigma_2)_{111} = \frac{E_2\Delta T}{1-\nu_2}\left[\frac{h_1E_1\alpha_1 + h_2E_2\alpha_2 + h_3E_3\alpha_3}{h_1E_1 + h_2E_2 + h_3E_3} - \alpha_2\right]$$

$$(\sigma_2)_{11} = \frac{E_2\Delta T}{1-\nu_2}\left[\frac{h_1E_1\alpha_1 + h_2E_2\alpha_2}{h_1E_1 + h_2E_2} - \alpha_2\right]$$

$$(\sigma_2)_{111} - (\sigma_2)_{11} = \frac{E_2\Delta T}{1-\nu_2}\left[\left(\frac{h_1E_1\alpha_1 + h_2E_2\alpha_2 + h_3E_3\alpha_3}{h_1E_1 + h_2E_2 + h_3E_3}\right)\right.$$

$$\left. - \left(\frac{h_1E_1\alpha_1 + h_2E_2\alpha_2}{h_1E_1 + h_2E_2}\right)\right] \qquad (6)$$

Depending on values of h_1, h_2, h_3, the oxide layer thicknesses; E_1, E_2, E_3, the elastic moduli of the various oxide layers; and on α_1, α_2, α_3, the thermal expansion coefficients of the oxide layers, equation (6) may yield either additional tensile or compressive stresses.

TABLE I

SURFACE STRAIN CORRECTION FACTORS

L = 2-1/64" $\quad \ell$ = 2-17/64" $\quad$ h = .03"

δ in.	Calculated Strain x 10^6	Actual Strain x 10^6	Correction Factor %
0 - .04	0 - 215	0 - 218	.05
.04 - .60	215 - 3224	218 - 3295	2.0
.60 - .75	3224 - 4030	3295 - 4225	4.5
.75 - .8	4030 - 4299	4225 - 5025	16.8
.8 - .85	4299 - 4568	5025 - 5742	25.5
.85 - .9	4568 - 4837	5742 - 6287	30.0
.9 - .95	4837 - 5105	6287 - 6895	35.0
.95 - 1.0	5105 - 5374	6895 - 7362	37.0
1.0 - 1.1	5374 - 5911	7362 - 7401	25.0
1.1 - 1.2	5911 - 6448	7401 - 7673	19.0
1.2 - 1.31	6448 - 7040	7673 - 8448	20.0

A. To determine actual strain, add % times calculated strain to calculated strain.

B. The correction factor was experimentally determined by comparing actual strain as measured by a strain guage with calculated strain. The error to a limited extent is caused by assuming small L/sR. The majority of error, however, is systematic in that the extensiometer used to measure δ exerts a downward force which depresses δ.

C. δ = 1.31 is the limit of the bending apparatus.

TABLE II

THERMAL EXPANSION COEFFICIENTS USED FOR CALCULATION OF MISMATCH STRAINS

	α Fe_3O_4	α 2-1/4 Cr - 1 Mo	α Fe_2O_3
50	10.72×10^{-6}	11.82×10^{-6}	10.96
100	11.38×10^{-6}	12.44×10^{-6}	11.14
150	12.03×10^{-6}	13.00×10^{-6}	11.22
200	12.68×10^{-6}	13.50×10^{-6}	11.45
250	13.33×10^{-6}	13.95×10^{-6}	11.55
300	13.97×10^{-6}	14.35×10^{-6}	11.82
350	14.62×10^{-6}	14.68×10^{-6}	11.90
400	15.26×10^{-6}	14.96×10^{-6}	12.15
450	15.9×10^{-6}	15.18×10^{-6}	12.23
500	16.54×10^{-6}	15.34×10^{-6}	12.45

(1) Coefficients for α Fe_3O_4 from Gorten relationship

$$\alpha_i = \frac{1}{a_o(T)} \left(\frac{da_o T}{dT}\right)$$

qhwew $a_o(T) = 8.3939 + 8.46 \times 10^{-5}T + 5.52 \times 10^{-8}T^2$.

(2) Coefficient for α 2-1/4 Cr - 1 Mo from Ref. 29 where

$\alpha \times 10^{-6} = 11.1392 + 1.41098 \times 10^{-2}(T) - 1.141258 \times 10^{-5}T^2$.

(3) Coefficient for α Fe_2O_3 from Gorten where $a_o = 5.0298$

$+ 5.30 \times 10^{-5}T + 1.12 \times 10^{-8}T^2$.

TABLE III

SPECIMEN IDENTIFICATION -- GROWING TIMES AND TEMPERATURE

Specimen #	Oxidation Temp (°C)	Exposure Time (hrs)	Expected Thickness (μm)	Expected Strain (%)
1-1	499°C (772°K)	506.34	8.89	.20
1-2	499°C	309.0	6.94	.225
1-3	499°C	78.25	3.49	.317
1-4	499°C	26.5	2.03	.416
1-5	499°C	5.67	.94	.612
2-1	403°C (676°K)	693.08	2.63	.366
2-2	403°C	449.25	2.12	.407
2-3	403°C	242.42	1.56	.475
2-4	403°C	113.5	1.07	.574
2-5	403°C	27.08	.52	.823

1. Expected thickness determined by using $h = 6.16 \times 10^{-3} \exp - \frac{14759}{RT} (t^{1/2})$.

2. Expected oxide fracture strain determined by using

$$\varepsilon^{\circ}_{f} = (\gamma/hE)^{1/2}$$

where $\frac{\gamma}{E} = 3.52 \times 10^{-11}$.

TABLE IV

OXIDE THICKNESS

Specimen #	Oxidizing Time (hrs)	Average Oxide Thickness (μm)	Maximum Oxide Thickness (μm)	Minimum Oxide Thickness (μm)
1-1	506.34	9.68	12.0	7.5
1-2	309.0	7.02	8.75	5.5
1-3	78.25	3.77	5.25	2.5
1-4	26.5	1.97	3.0	1.0
1-5	5.67	1.48	2.5	.5
2-1	693.08	4.06	5.25	3.0
2-2	449.25	3.19	4.5	2.0
2-3	242.42	2.39	3.0	1.5
2-4	113.5	1.15	1.4	.8
2-5	27.08	.60	1.0	.3

TABLE V

STRAIN TOLERANCE

Specimen #	Av. Oxide Thickness (um)	δ (in)	Corrected Mechanical Strain x 10^{-6}	Thermal Mismatch x 10^{6}	Total Strain (%)	
					Compressive Surface	Tensile Surface
1-1	9.68	1.14	7290	-139.5	-.743	.715
1-2	7.02	1.2	7674	-139.5	-.781	.753
1-3	3.77	1.16	7418	-139.5	-.756	.728
1-4	1.97	1.24	7996	-139.5	-.814	.785
1-5	1.48	1.28	8254	-139.5	-.839	.811
2-1	4.06	1.31	8448	-235.0	-.868	.821
2-2	3.19	--	--	-235.0	--	--
2-3	2.39	1.31	8448	-235.0	-.868	.821
2-4	1.15	1.31	8448	-235.0	-.868	.821
2-5	.6	1.31	8448	-235.0	-.868	

1. Thermal mismatch strain is the residual cooling strain in the oxide calculated using the thermal expansion coefficient values in Table II. Only the strain between the Fe_3O_4/metal interface has been used.

2. δ = 1.31" represents the maximum deflection of the straining apparatus. The fact that crack decoration revealed the presence of oxide cracks at this calculated tensile strain value indicates that cracking must have occurred at or before the total applied strain. The tensile strains, therefore, represent only an upper limit to the tensile strain required to crack the oxide.

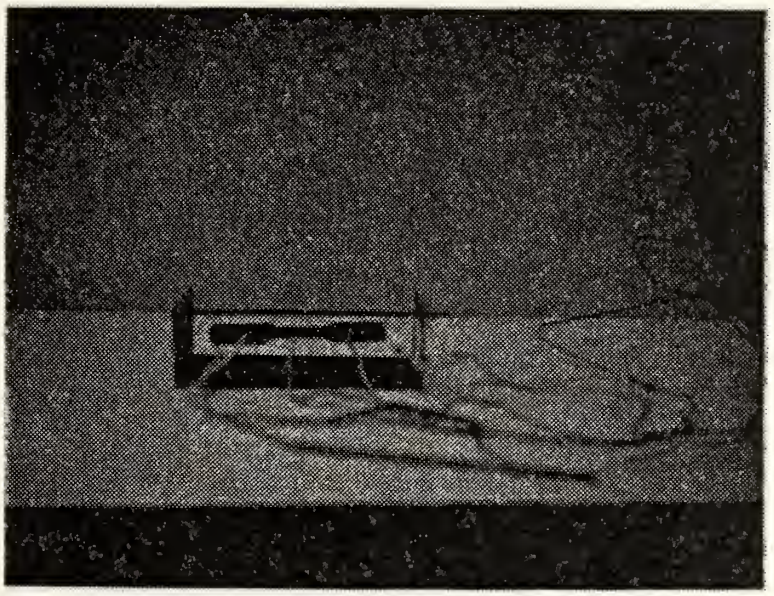

1. Length of Specimen = 5-1/2".

Figure 1: Suspended Specimen Sample Used for Furnace Variation Determination.

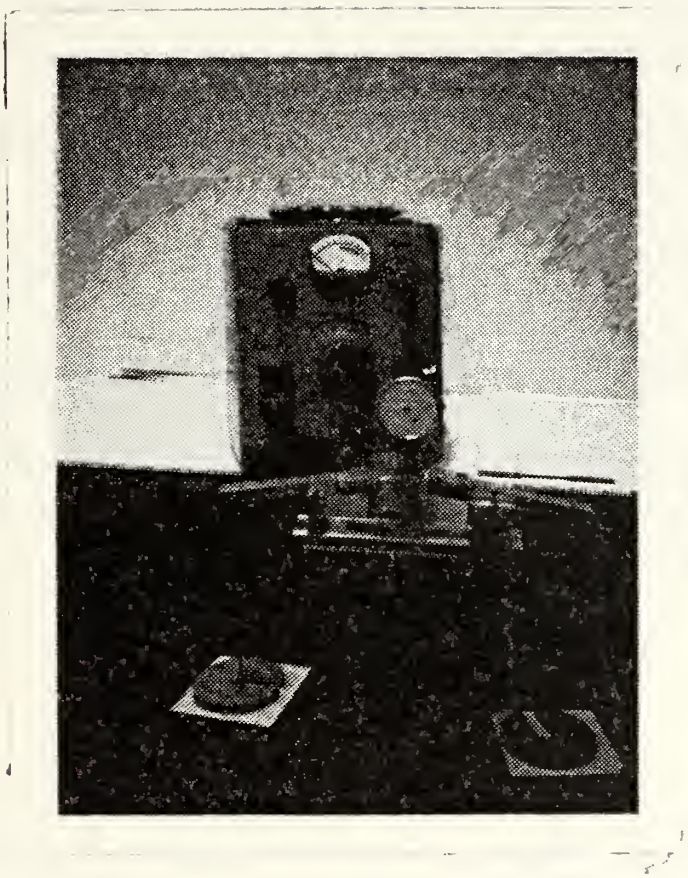

Figure 2: Straining Apparatus and Strain Indicator.

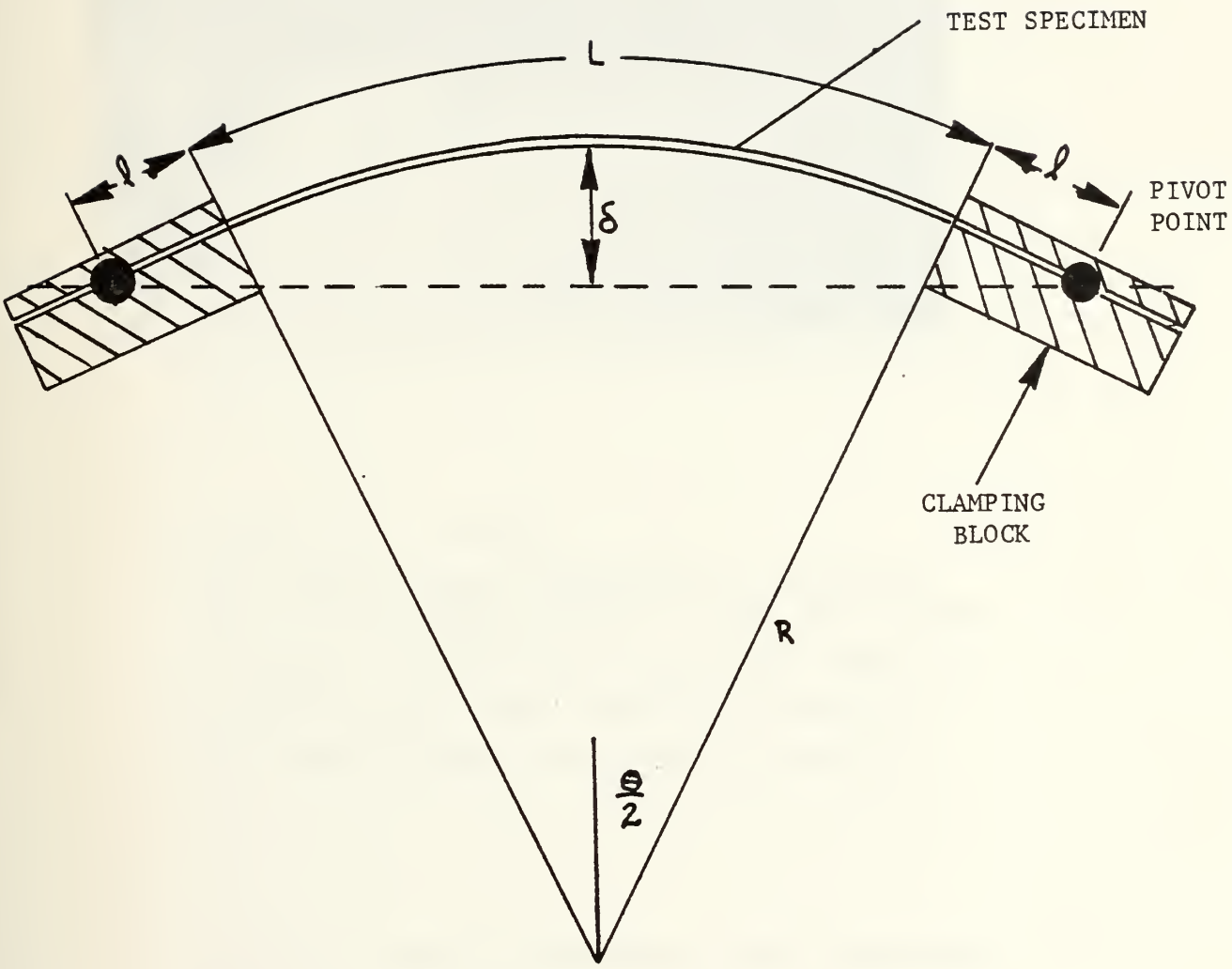

Figure 3: Geometry of Straining Apparatus

Specimen 1-1 1000X

White area is metal substrate. Dark gray layer is $(FeCr)_3O_4$ spinel. Light gray area is Fe_eO_4. Cloudy area above oxide layer is residual Fe_2O_3. Note oxide delamination with break through the $(FeCr)_3O_4$ layer.

Figure 4: Oxide Delamination 499°C Specimen.

Specimen 2-3 1000X

Lower white area is metal substrate. Upper white area is surface of retension clamp. Gray layer in center is oxide. Note absence of delamination.

Figure 5: Oxide Layer 403°C Specimen.

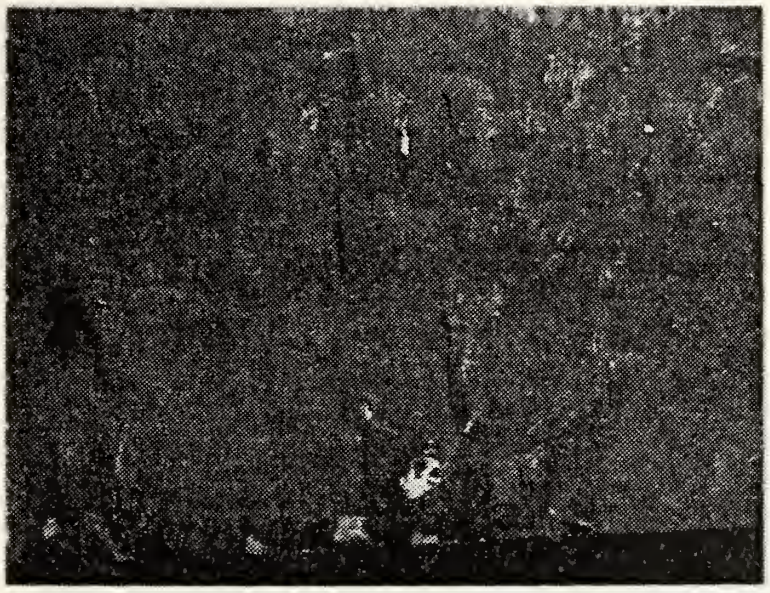

Specimen 1-2 1000X

Cracks normal to applied strain.

Figure 6: Tensile Surface Cracking

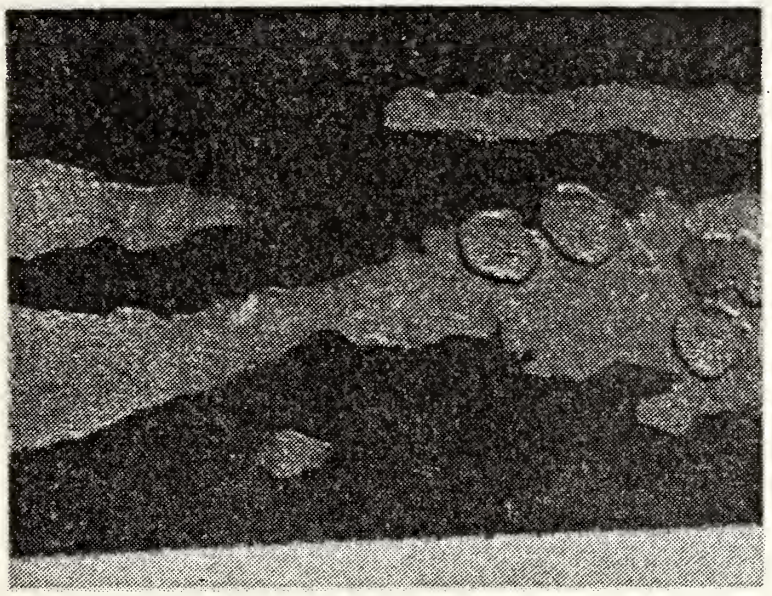

Spalling from compressive surface.

Figure 7: Compressive Surface Spalling.

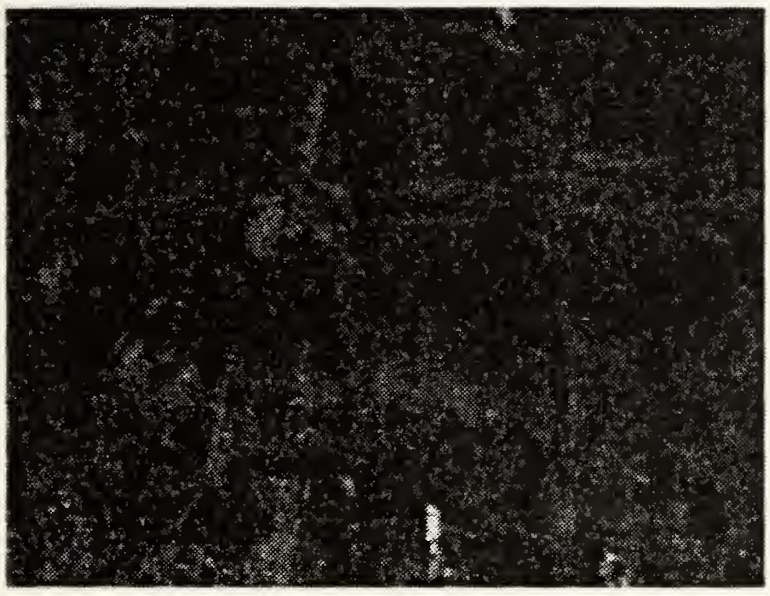

Specimen 2-1 1000X

Cracks normal to applied strain.

Figure 8: Tensile Surface Cracking.

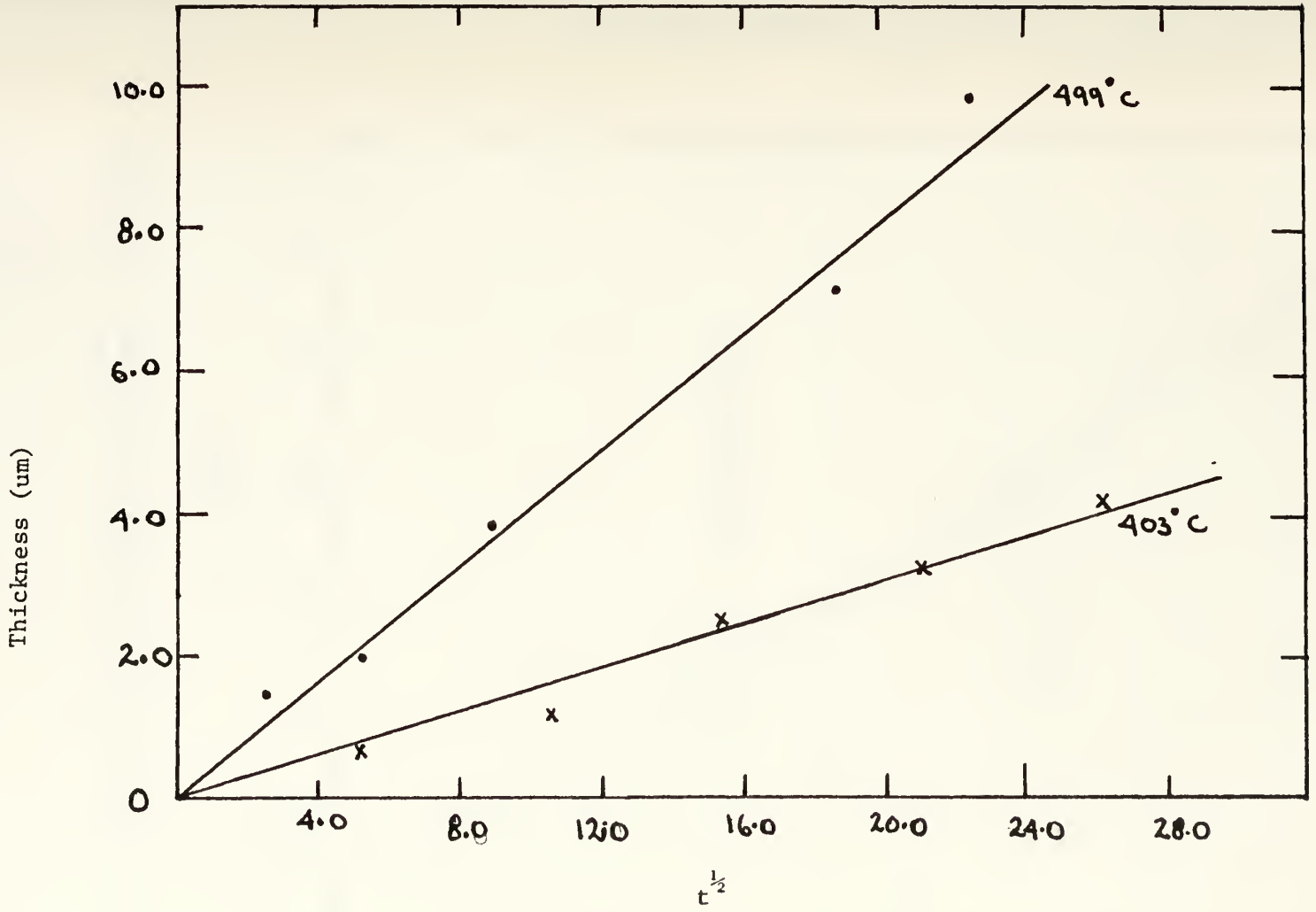

Figure 9. Average Oxide Thickness (um) Vs Time$^{\frac{1}{2}}$ (hrs)

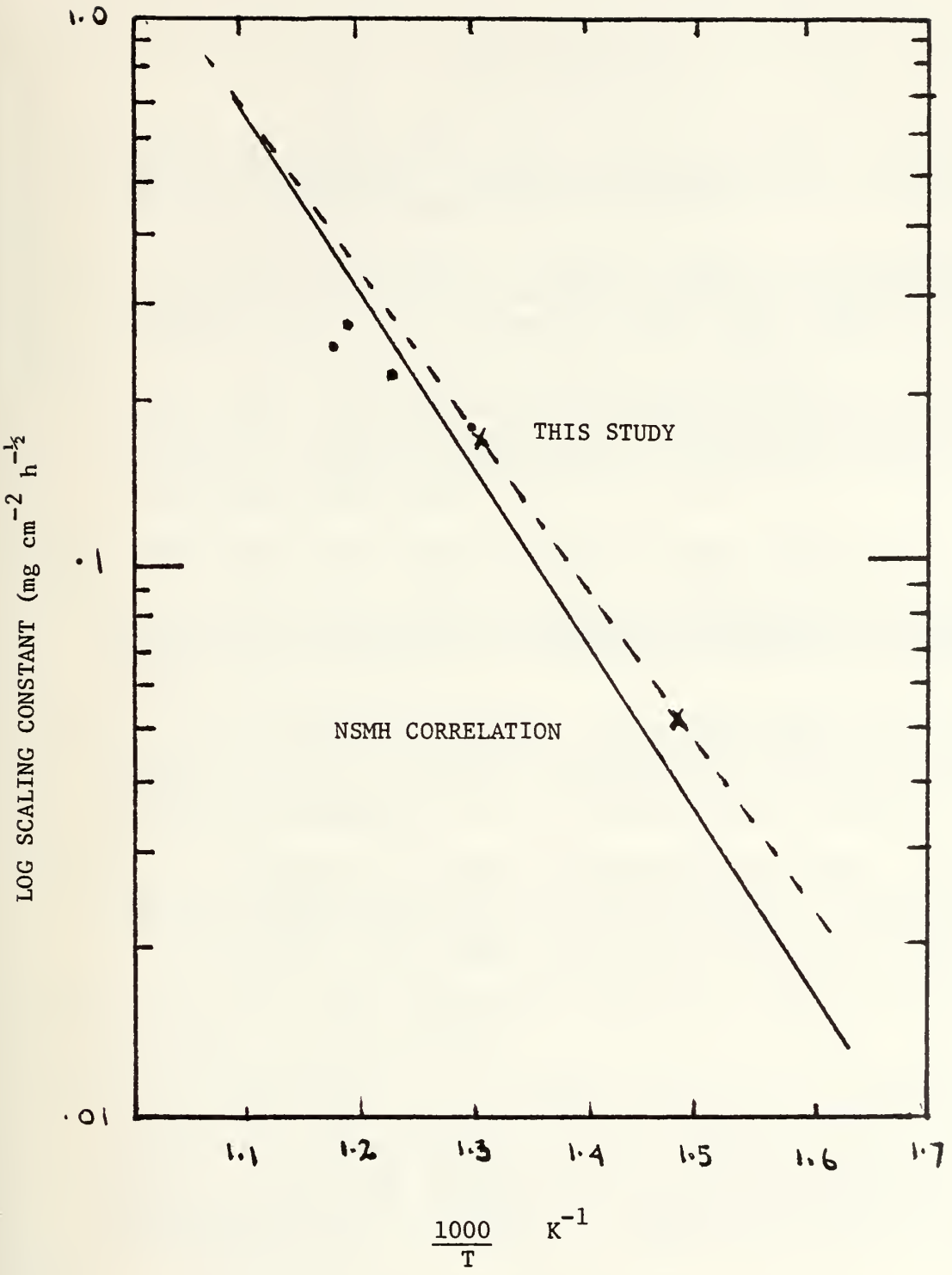

Figure 10. Comparison of Experimentally Determined Rate Constants with Published Data.

BIBLIOGRAPHY

1. Ronald W. Chickering, "The Nuclear Breeder: An Essential Energy Investment," Journal of Metals, Vol. 30, No. 2, pp 11-13, Feb. 1978.

2. J. W. Bennett and K. E. Horton, "Material Requirements for Liquid Metal Fast Breeder Reactors," Metallurgical Transactions, Vol. 9A, pp.143-149, Feb. 1978.

3. J. F. Copeland and G. J. Licina, "A Review of 2-1/4 Cr - 1 Mo Steel for LMFBR Steam Generator Applications," 1975 ASME - MPC 1, Symposium on Structural Materials for Service at Elevated Temperatures in Nuclear Power Generation, pp 55-84.

4. ASME Boiler and Pressure Vessel Code, Sections III and VIII.

5. J. R. Ellis and others, Elevated Temperature Fatigue and Creep Properties of Annealed 2-1/4 Cr - 1 Mo Steel, op cit. 3, pp 213-246.

6. C. R. Brinkman and others, "Time Dependent Strain Controlled Fatigue Behavior of Annealed 2-1/4 Cr - 1 Mo Steel for Use in Nuclear System Generator Design" Journal of Nuclear Material, Vol. 62, pp 181-204, 1976.

7. L. K. Severud, "Elevated Temperature Fatigue -- A Design Application Perspective with Directions for Improvements," 1976 ASME-MPC Symposium on Creep-Fatigue Interaction, R. M. Curran, Ed., ASME, MPC-3, pp 41-56, New York, 1976.

8. Rishi Raj, "Time Dependent Effects in Creep-Fatigue," op cit., 7, pp 337-343.

9. K. D. Challenger, A. K. Miller, and C. R. Brinkman, "Elevated Temperature Fatigue with Hold Time in a Low Alloy Steel-Creep Damage or Environmental Damage? Part I - Physical Mechanisms," to be published in Transactions ASME, Journal of Engineering Materials and Technology.

10. R. L. Klueh, "Heat Treatment Effects on the Tensile Properties of Annealed 2-1/4 Cr - 1 Mo Steel," Oak Ridge National Laboratory Report, ORNL 5144, May 1976.

11. R. L. Klueh, "Heat Treatment Effects on Creep and Rupture Behavior of Annealed 2-1/4 Cr - 1 Mo Steel," Metallurgical Transactions, Vol. 9A, Nov 1978.

12. K. D. Challenger, A. K. Miller, "Elevated Temperature Fatigue with Hold Time in a Low Alloy Steel: Creep or Environment Damage? Part II - Predictive Correlation," to be published in Transactions ASME, Journal of Engineering Materials and Technology.

13. Nuclear Systems Materials Handbook, Part 1, Group 2, Section 2. Property Code 4102, "Air-Side Corrosion," Revision 6-27-74.

14. M. I. Manning and E. Metcalfe, "Oxide Spalling in Stainless Steel Super-heater and Reheater Tubes and Possible Control Measures," Proceedings of the 6th European Corrosion Congress, Sept 1977, pp 121-127.

15. Mechanical Properties Test Data for Structural Materials, Progress Report for the Period Ending April 30, 1975, Oak Ridge National Laboratory, ORNL-5105, June 1975, pp 8-10.

16. Central Electricity Research Laboratories, Surrey, England, "The Spalling of Steam-Grown Oxide from Super-heater and Reheater Tube Steels," Electric Power Research Institute, EPRI FP-686, TPS 76-655, Final Report, Feb 1978, pp 1-9.

17. J. C. Griess, J. H. DeVan, and W. A. Maxwell, "Oxidation of Heated 2-1/4 Cr - 1 Mo Steel Tubing in Flowing Super-heated Steam," Oak Ridge National Laboratory, ORNL-5373, April 1978.

18. M. I. Manning and E. Metcalfe, "Oxidation of Ferritic Steels in Steam," International Conference on Ferritic Steels for Fast Reactor Steam Generators, British Nuclear Energy Society, London, May 1977, paper no. 63.

19. J. C. Griess, J. H. DeVan, and W. A. Maxwell, "Effects of a High Heat Flux on the Corrosion of 2-1/4 Cr - 1 Mo Steel in Super-heated Steam," Oak Ridge National Laboratory, ORNL/TM 555, Oct 1976.

20. A. T. Gorton, G. Bitisianes, and T. L. Joseph, "Thermal Expansion Coefficients for Iron and its Oxides from X-Ray Diffraction Measurements at Elevated Temperatures," Transitions of the Metallurgical Society of AIME, Vol. 233, pp 1519-1524, Aug 1965.

21. Walter D. Pilkey and Orrin Pilkey, Mechanics of Solids, QPI Series, 1974, p 269.

22. Op. cit., 21, p 330.

23. CRC, Standard Mathematical Tables, 25th Edition, p 143.

24. P. W. Atkins, Physical Chemistry, W. H. Freeman and Company, San Francisco, 1978.

25. C. E. Birchenall, "The Mechanism of Diffusion in the Solid State," Metallurgical Review, Vol. 3, pp 235-277, 1958.

26. Private Communication from Professor R. Newton to Professor M. Edwards, Naval Postgraduate School, Monterey, California.

27. Op. cit., 16, pp 4-13.

28. Robert E. Reed Hill, Physical Metallurgy Principles, Second Ed., D. Van Nostrund and Co., New York, 1973, pp 759-760.

29. D. L. McElroy, "Estimated Physical Properties of 2-1/4 Cr - 1 Mo Steel," Metals and Ceramics Division, Oak Ridge National Laboratory, Aug 9, 1974.

30. J. E. Castle and P. L. Surman, "The Self-diffusion of Oxygen in Magnetite. The Effect of Anion Vacancy Concentration and Cation Distribution," Journal of Physical Chemistry, 1969, Vol. 73, Part 1, pp 632-634.

31. Tifeffertz H. Nisel, Alliantz/Berichte, Vol. 16, Apr 1971.

INITIAL DISTRIBUTION LIST

		No. Copies
1.	Defense Technical Information Center Cameron Station Alexandria, Virginia 22314	2
2.	Library, Code 0142 Naval Postgraduate School Monterey, California 93940	2
3.	Department Chairman, Code 69 Department of Mechanical Engineering Naval Postgraduate School Monterey, California 93940	1
4.	Asst Professor K. Challenger, Code 69 Mc Department of Mechanical Engineering Naval Postgraduate School Monterey, California 93940	5
5.	Major Robert Lawrence Langdon Unit 6 58 Cassandra Boulevard Don Mills, Ontario, Canada	3

189362
Thesis
L2627
c.1
Langdon
Calculation of the oxide growth rate of 2-1/4 Cr - 1 Mo steel in air and the subsequent measurement of the strain required to crack the oxide.

Thesis
L2627
c.1
189362
Langdon
Calculation of the oxide growth rate of 2-1/4 Cr - 1 Mo steel in air and the subsequent measurement of the strain required to crack the oxide.

thesL2627
Calculation of the oxide growth rate of
3 2768 002 11330 0
DUDLEY KNOX LIBRARY